Materials & Design 206 (2021) 109791

Contents lists available at ScienceDirect

Materials & Design

journal homepage: www.elsevier.com/locate/matdes

# Ultrafast electrohydrodynamic 3D printing with *in situ* jet speed monitoring

Ievgenii Liashenko [a,b], Alberto Ramon [a], Andreu Cabot [a,c,*], Joan Rosell-Llompart [b,c,*]

[a] Catalonia Institute for Energy Research - IREC, Jardins de les Dones de Negre 1, 08930 Sant Adrià de Besòs, Barcelona, Spain
[b] Department of Chemical Engineering, Universitat Rovira i Virgili, Av. dels Països Catalans 26, 43007 Tarragona, Spain
[c] Catalan Institution for Research and Advanced Studies – ICREA, Pg. Lluís Companys 23, 08010 Barcelona, Spain

## HIGHLIGHTS

- We demonstrate a new way to determine speed of electrohydrodynamic jets *in situ* during printing.
- Our strategy is based on electrostatic jet deflection.
- Our method enables combining submicrometer resolution with high printing speed.

## GRAPHICAL ABSTRACT

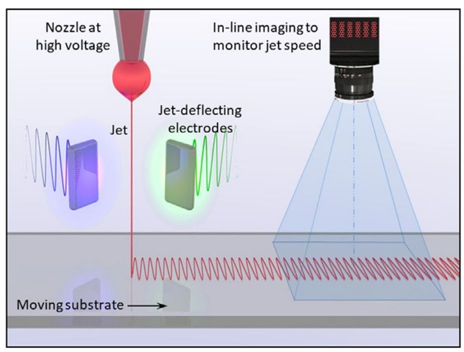


## ARTICLE INFO

*Article history:*
Received 29 December 2020
Revised 28 April 2021
Accepted 2 May 2021
Available online 4 May 2021

*Keywords:*
Additive manufacturing
Near-field electrospinning
Nanofiber
Jet speed
Electrohydrodynamic jet

## ABSTRACT

Additive manufacturing by near-field electrospinning is based on the continuous deposition of a nanofiber on a substrate. Owing to the small fiber size and the high jet speeds that can be achieved, this method potentially combines submicrometer resolution with high printing speed. Printing with high fidelity depends critically on controlling the jet arrival speed, which must be matched to the printing speed. Unfortunately, current methods to determine the jet speed are cumbersome and cannot be performed *in situ* as they are based on laborious high-resolution imaging of individual nanofibers. Using inexpensive optical equipment, here we demonstrate a new way to determine the jet speed *in situ* during printing. Our strategy is based on electrostatic jet deflection, in which the speed is readily computed from the width of a printed object made from a periodically printed motif. Such width can be easily obtained inline by optical inspection, overcoming the need to resolve individual nanofibers. This information can be used to feedback control the printing process. The proposed approach will not only assist in studying the fundamental relation between the jet speed and other printing parameters, but also enable reproducible printing of fibers in a rapidly expanding area of applications.



## 1. Introduction

Submicrometer electrohydrodynamic (EHD) jets deposited as continuous nanofibers allow extending cost-effective ink- and melt-based printing technologies into the nanoworld. Such EHD jet printing has shown promise in the making of flexible electron-

* Corresponding authors at: Catalan Institution for Research and Advanced Studies – ICREA, Pg. Lluís Companys 23, 08010 Barcelona, Spain.

*E-mail addresses:* acabot@irec.cat (A. Cabot), joan.rosell@urv.cat (J. Rosell-Llompart).

https://doi.org/10.1016/j.matdes.2021.109791
0264-1275/

ics circuits, energy storage microdevices, acoustic sensors, metamaterials, biomaterials, artificial human tissues, and structures in various fields of application [1–8]. An EHD jet is formed when electrostatic forces strongly pull on a liquid drop, rupturing it. Often, the drop adopts a pointed shape, known as Taylor cone, which ejects the EHD jet (Scheme 1) [9]. The electrostatic charging at the liquid–gas interface overcomes the droplet size limitations resulting from surface tension in classical nozzle-based printing methods, thus allowing the printing of objects having much smaller voxel sizes [2,10]. Hence, the EHD jet's thickness can be significantly smaller than the nozzle diameter, down to the 100 nm scale, and is unrelated to it [11]. In addition, viscous and elastic stresses stabilize the jet against the development of Rayleigh jet breakup. When using viscoelastic inks, typically containing polymers, the jet is usually printed as an unbroken, continuous line. This method of printing is known as near-field electrospinning (NFES) [12], for its connection to electrospinning [13], as EHD direct-writing [1], or as melt electrowriting (MEW) when a melt is used instead of a solvent-based ink [6]. Lines in the micrometric and sub-micrometric range can easily be printed in this way [1,14].

Since the jet is electrostatically attracted towards the substrate, its arrival speeds can be substantially higher compared to extrusion-based printing [15,16], ranging from mm $s^{-1}$ for MEW/NFES to dozens of m $s^{-1}$ for solution electrospinning [6,12,13]. Knowing the jet speed is critical for controlling the printing process and obtaining the best printing fidelity, but its measurement poses a huge practical challenge due to the jet's thinness and its high speed [17,18]. Scheme 1a shows how jet speed influences the printed fiber pattern for the conventional stage-driven printing mode, in which the collection substrate is translated under the jet by a mechanical stage. Three regimes are found depending on the speed of the jet. In stage-driven printing, obtaining pattern fidelity relies on matching the (horizontal) substrate speed $U_s$ (relative to the nozzle) to the (vertical) jet arrival speed $U_j$ attained by the jet right before it reaches the substrate (Scheme 1a, center panel). At substrate speeds exceeding the jet speed, $U_s > U_j$, stage-driven printing enters the *stretched jet regime*, in which the jet is under tension while stretching. Here, the printed pattern deteriorates, although it can still be used to print lines and walls with a large curvature radius (large compared to the fiber diameter) [19,20]. Stage-driven printing with $U_s$ set below $U_j$ ($U_s < U_j$) leads to the *buckled jet regime*. Here, the EHD jet is under compression next to the substrate, undergoing buckling instabilities. Such instabilities can result in different printed patterns depending on the ratio $U_s/U_j$: sinuous folding, zigzag folding, helical coiling, meandering/serpentine, etc. [11,21]. Such instabilities resemble those experienced by gravitationally driven jets impinging on a moving belt, wherein a liquid "rope" on reaching the collection substrate develops axial compressive stresses and becomes unstable to bending [22,23]. As the amplitude and wavelength of the printed coils can be quite small (from a few to several tens of microns), this regime has been proposed for printing flexible electronics [21,24]. However, only the patterns allowed by the physics of the buckling are available. In addition, precise fiber positioning is not, strictly speaking, achieved because the buckling decides the trajectory of the jet near the substrate. Furthermore, although the printed patterns can be periodic, chaotic buckling frequently sets in [25].

The approaches for determining the jet speed in stage-driven printing are based on the use of microscopy for imaging the fiber pattern after printing, with too slow a feedback cycle. For example, the jet speed has been determined by inspection of printed lines taken at different substrate speeds at three different regimes (Scheme 1a), and the samples are inspected by microscopy to identify the moment when the wavy printed pattern becomes a straight line [24,26,27]. At this "matched-speed" condition, the stage speed equals the jet speed. This approach relies on resolving individual fibers to ensure the straight-line condition, which involves the use of a microscope able to resolve the jet's small size (in the micrometer to sub-micrometer ranges), typically a scanning electron microscope. Even when the fibers are large enough to be visible to the naked eye, such as in MEW [28,29], this approach requires iterations before the jet speed can be determined.

In another approach, a printed pattern is analyzed to extract the fiber length printed within a time interval, thus a given travel of the collection surface [17,27]. The jet speed is then computed as

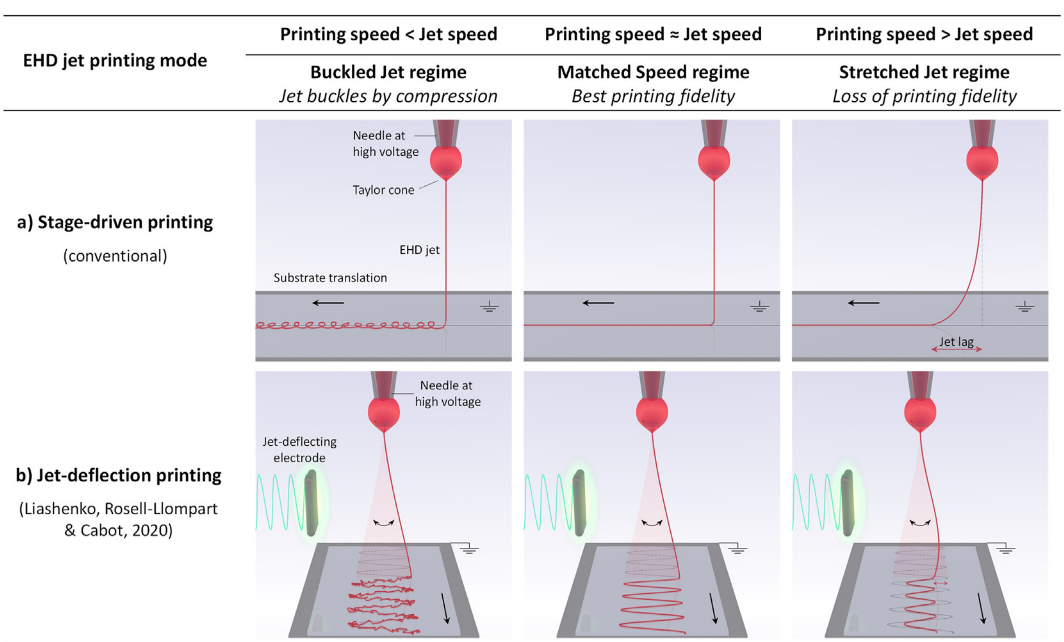


**Scheme 1.** Classification of printing regimes of electrohydrodynamic (EHD) jet-based printing for (a) conventional stage-driven printing mode, and (b) jet-deflection printing mode.

the length divided by the time. Here also, a powerful microscope is needed to resolve the individual fiber. In addition, this approach only works if the fiber overlaps with itself infrequently, which is not always fulfilled.

Therefore, despite many achievements in EHD jet printing, we still lack robust strategies for rapid *in situ* determination of the jet speed. On the other hand, theoretical modelling is still unable to reliably predict the jet speed, because of the complex dependence of jet dynamics on fluid properties, which vary along the jet. Thus, simpler *in situ* approaches to determine EHD jet speed are needed. Ideally, such approaches should be interfaceable with fast pattern-recognition software, so they can be implemented in commercial products and industrial settings.

To overcome the printing speed limitations imposed by the use of mechanical stages, we recently introduced a EHD jet-deflecting printing technology based on the rapid electrostatic stirring of the EHD jet (Scheme 1b) [10]. The trajectory and point of arrival of the jet to the substrate are controlled by voltages applied to additional ('jet-deflecting') electrodes, allowing jet stirring at very high accelerations, up to $5{\cdot}10^5$ m s$^{-2}$. Therefore, ultrafast printing speeds are possible compared to stage-driven printing [10]. The jet deflecting parameters are programmed to ensure matching between the jet speed and the desired *printing speed* (namely, the speed of the contact point over the substrate). At this condition, the jet is neither under compression nor under tension (Scheme 1b, center panel). Unlike in stage-driven printing, the position of the contact point where the fiber meets the substrate is controlled independently from the motion of the substrate, which can even remain still.

In the present work, we propose applying jet-deflecting to determine *in situ* the EHD jet speed without resolving the individual fiber, but from the much larger size of a printed pattern. A key advantage of this strategy is that the printed fiber track is much wider than the fiber; therefore, it can be observed and quantified easily using standard optical inspection equipment. We demonstrate this by two approaches. (1) In the first one, the EHD jet is continuously deposited on a moving collector while it is electrostatically deflected periodically in the transverse direction (as shown in Scheme 1b). The width of a printed track with a repeating motif can readily be converted to the jet speed from knowledge of the printed pattern geometry and the frequency of the jet deflection signal. (2) Our second approach is based on building a 3D structure, layer by layer over a motionless substrate. In this case, the jet speed is obtained from the signal frequency and the width of the object of known shape. For convenience, we focus here on inks, but the same strategies could be translated to the case of melts.

## 2. Methods and materials

### 2.1. Printing setup

Our EHD printer comprises a thin tube as nozzle, a glass syringe holding the printing ink (Hamilton #81320, 1 ml), a syringe pump (Harvard apparatus, Pump 11 Pico Plus Elite 70-4506) to supply the ink from the syringe to the nozzle at a known rate, an XY translation mechanical stage (PI miCos linear stages PLS-85 with 10 mm range in both X and Y with RS422 encoders) to hold the printing substrate, and a high voltage power supply (Matsusada AU-20P15) providing (in our case) positive high voltage to the nozzle (Fig. 1a). In addition to these standard elements, our printer has extra electrodes around the jet (Fig. 1a, d) for modifying the electric field in the vicinity of the jet, to deflect it from its otherwise vertical trajectory. Two steel electrodes with size (height, width and thickness): 10 × 3.0 × 0.5 mm were used at 90° from one another as shown in Fig. 1d, positioned 10 mm away from the nozzle-axis. In this configuration, they were glued to a plastic holder made with an SLA 3D printer (Formlabs Form 2) using FLGPCL04 clear resin while the electrode to substrate distance was fixed at 1 mm. The printing substrate is attached atop an Earth-grounded aluminum plate, which is mounted on the XY translation stage. As nozzles, we either used stainless needles with blunt ends (Hamilton N726S, 26 s gauge, 127 μm ID, 474 μm OD) or borosilicate glass tips (c.a. 150–200 μm OD), as detailed in SI, Table S1. No surface treatment was applied to their ends. The glass tips were manufactured by pulling borosilicate glass tubing (Sutter Instruments, B100-50-15; 1.0 mm OD, 0.50 mm ID) using a Pipette puller (Sutter Instruments P-97) and manually breaking the tips by scratching two tips against each other. The large (tubing) end of the glass tips was glued atop of a stainless-steel needle with blunt end (B Braun Sterican, 27 gauge; 0.47 mm OD). As practiced conventionally, our 3D printing was controlled through the parameterization of the layer-by-layer deposition process to print an object with predefined geometry, size, and microstructure. A custom-made code, developed in LabVIEW, and a data acquisition card (DAQ card, National Instruments USB-6259) generated the jet-deflecting electrodes voltages, defined as a function of the geometry of the predesigned pattern, the layer printing frequency and the signal amplitude. Synchronized analog signals (max. ± 10 V) provided by the DAQ card were amplified (max. ± 2000 V, with Matsusada AMJ-2B10 and Trek 677B amplifiers) and applied to the jet-deflecting electrodes typically within 1000–2000 V for 10 mm nozzle-to-electrodes separation. The nozzle voltage was also monitored through the LabView software, while camera imaging and the XY stage motion were controlled through manufacturer's software.

### 2.2. Materials and inks preparation

Polyethylene oxides (PEO) of various molecular weights were purchased from Sigma-Aldrich (#182001, viscosity-average molecular weight 300 kDa; #372781, 1 MDa; #189472, 5 MDa). Poly(3,4-ethylenedioxythiophene) polystyrene sulfonate (PEDOT:PSS) dispersion was purchased from Sigma-Aldrich (#655201, 3–4% in water). Ethanol and ethylene glycol were reagent grade from different sources. All chemicals were used as received without further purification. Ag nanoparticles of diameter ca. 50 nm were synthesized using PVP as surfactant [30]. After synthesis, the nanoparticles were thoroughly washed by multiple precipitation and redispersion cycles using ethanol as solvent and acetone as antisolvent, and finally, were precipitated for posterior use. The thus obtained Ag nanoparticles could be dispersed in polar solvents such as water and ethanol. For inks formulation, deionized water was the main solvent, to which some amounts of ethanol or ethylene glycol were added to lower surface tension and evaporation rate during printing. PEO inks were prepared by dissolving PEO (typically 2–10 wt%) in the solvent mixture for 24 h under magnetic stirring. PEDOT:PSS inks were prepared by adding the proper amount of PEDOT:PSS dispersion into the PEO ink and homogenizing the mixture by magnetic stirring. Ag nanoparticle inks were prepared by adding the PEO ink into a flask containing precipitated Ag nanoparticles and dispersing them using ultrasonication and magnetic stirring. Ink compositions, resulting fiber diameters and corresponding printed structures are specified in the SI file, Table S1. All inks were kept in sealed vials, where they could be stored for months without showing signs of degradation. PEDOT:PSS inks were stored at 4 °C.

### 2.3. Printing protocol and in situ inspection

Silicon wafers (University Wafers #452, p-type, ⟨100⟩) were used as substrates. Silicon was cleaned with isopropanol to remove organic contamination prior to printing. The substrate was either

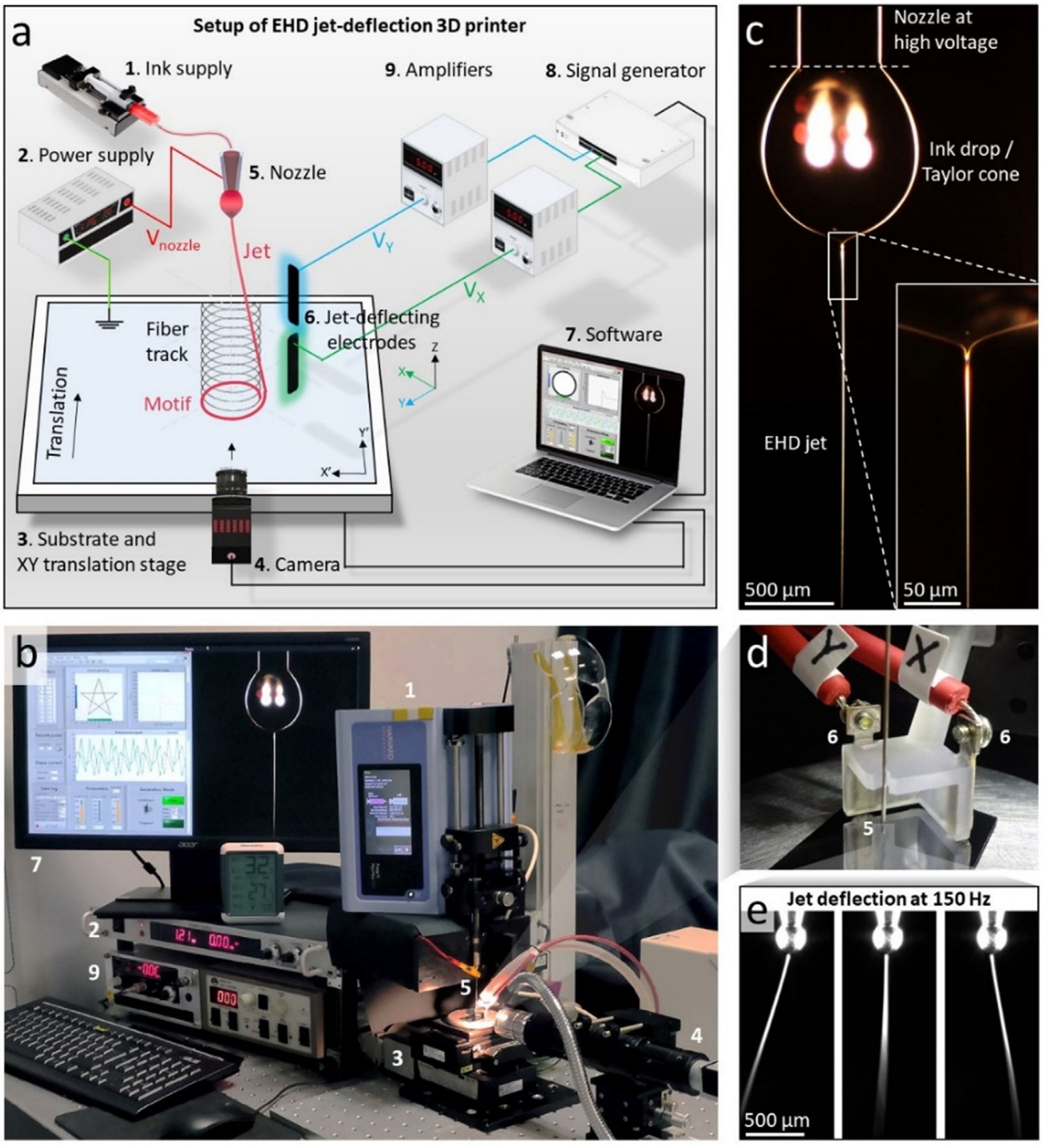


**Fig. 1.** The electrostatic control of the jet trajectory. (a) Setup schematic and (b) photograph of our EHD jet printer with jet-deflecting electrodes. (c) Dark field optical photographs of the nozzle, ink drop forming a Taylor cone, and (inset) the electrified jet generated by applying 1000 V between the nozzle and a printing substrate. (d) Set of two jet-deflecting electrodes and needle used as nozzle. (e) High-speed video captures of a jet at the leftmost, center, and rightmost positions while being deflected at 150 Hz with two opposing electrodes positioned 3 mm away from the nozzle axis, for a nozzle-to-substrate distance of 5 mm. Ink: 5% PEO 300 kDa in water:ethanol (1:3).

translated continuously to print 2D fiber tracks, or only moved in steps between which the substrate remained motionless while 3D structures were printed by electrostatic jet deflection. The separation between the nozzle exit and the printing substrate was set at 3 mm, unless otherwise noted. Inks were loaded into the glass syringe and supplied to the nozzle with a typical flow rate of 0.05–0.07 μl min$^{-1}$. The pendant drop formed at the nozzle aperture. Upon application of a high voltage to the nozzle, the ink drop forming at the exit of the nozzle expels a charged jet toward the substrate (Fig. 1c), whose thickness is independent of the size of the nozzle aperture. EHD jetting was initiated by slowly increasing the nozzle voltage up to 1800–3000 V, until the pendant ink drop forming at the exit of the nozzle elongated and fell on the printing substrate, establishing a jet. This voltage was then lowered to 800–1500 V typically, and the jet was stabilized for 2 min before initiating the printing. The printing process was carried out under ambient temperature in the range 18–20 °C. Where noted, a gentle, laminar flow of dry nitrogen gas was supplied around the jet from a side tube to ensure predictable solvent evaporation rate. The printing process was monitored with a CMOS camera (Basler acA2040-25gc) mounted on an optical microscope, which consisted of a 12x lens with adjustable zoom and focus (Navitar 1-50486), a 2x lens adaptor (Navitar 1-62136), and a 5x microscope lens (Mitutoyo 1-60226), resulting in nominal working distance of 34 mm. The optical axis was set horizontal. A fiber optic illuminator (AmScope HL-250-A) on the other side of the observed object aimed at it at ca. 5° angle from the microscope optical axis, so that direct light did not reach the camera sensor for dark-field setting (as on Fig. 1c). For real-time monitoring of the liquid drop during the printing process, a paper sheet was used as a diffuser, placed between the light source and the observed object for bright-field setting. For obtaining high-speed captures shown in Fig. 1e, the CMOS camera was substituted with a high-speed video camera (Photron FASTCAM-1024PCI).

### 2.4. Fiber inspection

In jet-deflection printing, either fiber tracks were printed as the substrate is moved, or 3D structures were printed with the still substrate. These tracks and 3D structures were inspected after printing by scanning electron microscopy (SEM), confocal microscopy, and macro-photography to simulate *in situ* machine-inspection. SEM micrographs were obtained at 1–2 kV electrons acceleration voltage on AURIGA (FIB-FESEM) from Carl Zeiss using either an in-lens detector or a secondary electrons (SE2) detector. Before imaging any samples by SEM, they were sputter-coated with silver to a several nm using a DC magnetron sputter (Emitech K575X, 80 mA, argon, 90 s) while the sample was slowly rotated to obtain uniform thickness. This improved the quality of SEM images and protected the PEO fiber from degradation/shrinkage caused by the electron beam. Confocal microscopy images were taken using a Sensofar PLu Neox confocal microscope with polarized light to improve the contrast between printed fibers and substrate. Confocal images larger than 0.5 mm were obtained by stitching multiple images having a smaller field of view, which was done within the original Sensofar software. To simulate machine-inspection imaging of printed fiber tracks, PEO fiber tracks collected as the substrate is moved were imaged after printing using the same CMOS camera and microscope assembly that was used for *in situ* inspection.

### 2.5. Electric field simulation

The simulation of the electric potential and field around the jet in the presence of a single jet-deflecting electrode was done in COMSOL Multiphysics® 5.2a using the following parameters: nozzle potential at +1000 V; substrate was kept at 0 V (Earth grounded) and jet-deflecting electrode at −50 V; nozzle-to-substrate separation of 3.6 mm; and nozzle axis-to-electrode separation of 2 mm.

## 3. Results and discussion

### 3.1. Printing setup

Our EHD printer comprises a thin stainless steel or borosilicate glass tube as nozzle, a glass syringe holding the printing ink, a syringe pump to supply the ink from the syringe to the nozzle, an XY translation mechanical stage to move the printing substrate, and a high voltage power supply providing positive high voltage to the nozzle (Fig. 1a, see methods section for details). Upon applying a high voltage to the nozzle, the ink drop forming at the exit of the nozzle expels a charged jet toward the substrate (Fig. 1b). The jet width is independent of the size of the nozzle aperture and it can be as low as 100 nm and below depending on the ink properties, the supply rate and the applied voltage [31]. The inks used consisted of a 2–10 wt% dissolution of PEO in water and contained some amounts of ethanol or ethylene glycol to lower surface tension and evaporation rate during printing. Inks incorporating PEDOT:PSS and 50 nm silver nanoparticles were also used (see methods section for details).

In addition to these standard EHD printing elements, our printer had extra electrodes around the jet (Fig. 1a, d) for modifying the electric field in the vicinity of the jet, to deflect it from its otherwise vertical trajectory. We used two electrodes placed at 90° to one another, as shown in Fig. 1d, and applied voltages typically within the range 1000–2000 V. When using only two jet-deflecting electrodes, the printing of symmetric patterns usually required corrections by software (see supplementary information for a discussion on the use of 1, 2 and 4 jet-deflecting electrodes). Supplementary Fig. S1 shows the electric field distortion created by a single jet-deflecting electrode. In this simulation, a massless jet is shown as an electric field "streamline" (in white) starting at the tip of Taylor cone, along with the electric potential and the electric field (arrows) around the jet. Color gradient represents the electric equipotential lines and black arrows represent the electric-field vectors, of length proportional to field strength. The deflecting electrode, nozzle and ink drop were plotted in white for clarity but are at the specified potentials. Fig. 1e shows high-speed video captures of the thin jet oscillating upon the action of symmetrically alternating signals applied to two electrodes. A custom-made code and a data acquisition card were used to generate the jet-deflecting electrodes voltages, defined as a function of the size and geometry of the predesigned pattern. Through the parameterization of the layer-by-layer deposition process, three dimensional (3D) patterns and objects with predefined geometry, size, and even microstructure could be also printed [10]. The substrate, typically a silicon wafer here, was either translated continuously to print two-dimensional (2D) fiber tracks, or only moved in steps between which the substrate remained motionless while 3D structures were printed by electrostatic jet deflection.

### 3.2. Determining jet speed from 2D patterns

In the conventional method, Fig. 2a, the stage is translated at increasing speeds, from a value lower than the jet speed, until the *matched speed regime* is found (Scheme 1). At the lower stage speeds, the jet buckles onto the substrate, printing loops. The amplitude of the loops reduces at increasing stage speeds, eventually changing to a serpentine pattern made of meanders whose amplitude decreases as the stage speed keeps increasing. Eventually, a straight fiber forms when the stage speed matches or exceeds the jet speed (Fig. 2a, bottom panel). In the latter case, the jet is stretched by tension transferred from the contact point of the jet with the substrate (*stretched jet regime*, Scheme 1). This method is based on searching for the critical condition at which the jet first becomes straight. Unfortunately, a straight jet is still obtained when the jet speed is exceeded by the stage speed. Therefore, increasing the accuracy of the jet speed determination is difficult. Another disadvantage is that a fast (and fast-accelerating) stage is needed (at least as fast as the jet), where this could be a challenge because EHD jets in NFES regime can attain speeds well above 1 m $s^{-1}$. In addition, a powerful microscope is needed to precisely resolve a single fiber on the printed substrate, enough to distinguish a perfectly straight fiber from meandering fibers with a low amplitude. As a result of these shortcomings, the inline implementation of the conventional method seems exceedingly complex.

We propose a new approach based on analyzing printed patterns obtained with substrate translation while periodically deflecting the jet transversely to the stage translation to print a repeating pattern, or motif (Fig. 2b). The jet speed is determined by dividing the length of fiber $L$ printed in one period of jet deflection by one period $T$ (the inverse of the applied frequency $\nu$ of the jet deflecting signals). This determination does not require a fast stage and is nearly independent of stage speed. As the substrate speed increases from a low value, the pattern's amplitude decreases while its wavelength increases (Fig. 2b, panels A through F). When the substrate speed exceeds the jet speed, the fiber becomes straight (Fig. 2b, panel G), just as in the conventional method. The key advantage of this method lies in the fact that all of the generated patterns shown in Fig. 2b except panel G can be used to compute the jet speed from the known predefined geometry of the printed pattern. In this example, sawtooth waves are created, so the jet speed ($U_j$) can be obtained from the measured

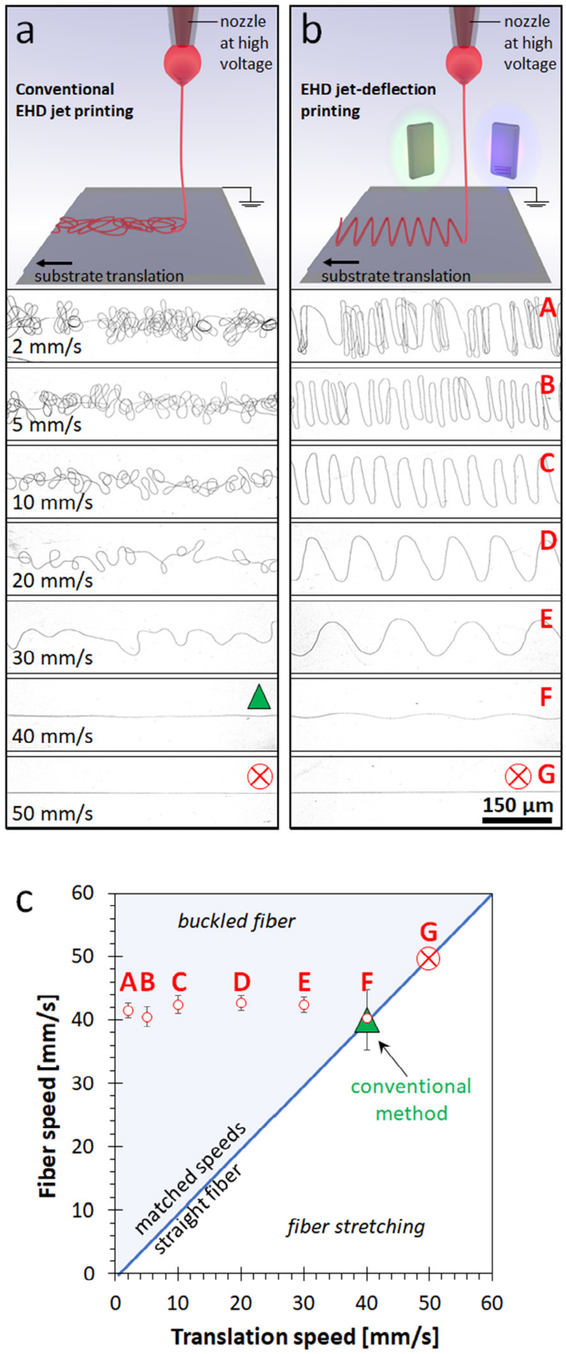


**Fig. 2.** Comparison of conventional and jet-deflection methods for determining the fiber speed. (a) Conventional method: Schematic and SEM images of a PEO fiber collected at different substrate speeds. The stage speed matches the jet speed when straight fiber is printed. (b) Jet-deflecting method: The jet is electrostatically deflected perpendicularly to the substrate translation at 200 Hz with 1200 V signal amplitude. The jet speed is determined from the width of the printed pattern at any stage speed. (c) Jet speed determined by the conventional method (green triangle) and by the jet-deflection method (circles). Error bars are obtained from the standard deviation computed from 3 to 5 data points for each translation speed. Ink: 7 wt% PEO 300 kDa in 1:1 vol water/ethanol. Syringe pump rate: 70 nL min$^{-1}$. Metal nozzle at 1500–2000 V. SEM images obtained using in-lens detector and shown in negative for better contrast. (For interpretation of the references to color in this figure legend, the reader is referred to the web version of this article.)

width of the fiber motif track ($W$), the stage speed ($U_s$) and the jet-deflecting frequency ($\nu$):

$$U_j = L/T = 2\nu\left[W^2 + (U_s/(2\nu))^2\right]^{1/2} \quad (1)$$

The jet speeds computed from the panels in Fig. 2b are shown in Fig. 2c. The consistency of the jet speed data determined at different stage speeds proves that the stage motion did not impart speed to the fiber, as assumed in the calculation. Alternative oscillating signals and a more sophisticated formula could be used to improve accuracy, by factoring in the fiber curvature radius.

The proposed jet deflection approach overcomes the above-mentioned difficulties of the conventional methods, as it neither requires matching speeds nor resolving individual fibers. Nor is a fast stage needed. In fact, the proposed method works better at low stage speeds, where the accuracy on the track's width will be better. In addition, a single pass suffices in the new approach, in contrast to the conventional method, where many passes are needed to find the critical *matched speed regime* condition. Finally, the required stage travel is much smaller in our method as the stage can be moved much slower than the jet. In the conventional method, the substrate may need to travel several millimeters or more, while accelerating up to the jet speed, and then decelerate back to zero. For instance, for an acceleration of 20–30 m s$^{-2}$ typical of a high-performance stage, reaching 0.5 m s$^{-1}$ would require acceleration/deceleration travel of at least 4–6 mm, giving a total travel of at least 20 mm.

Finally, note that in panel B of Fig. 2b the fiber is more regularly distributed than in panel A, where the density of fibers is less homogeneous. This happens by the tendency of the fibers to fall on top of previously deposited ones due to electrostatic attraction. Such attraction is the result of the charge reversal taking place after deposition caused by electrostatic induction [10,32]. This phenomenon has no impact on the determination of speed, because the width of the track is not affected.

### 3.3. Jet deflection strategy based on 3D structures

The idea for obtaining the jet speed from a printed track and a jet deflection signal of known frequency can be extended to the case where 3D structures are printed by periodically stacking layers of fibers. Electrostatic charge dissipation and charge reversal here become key in promoting the precise self-assembly of the fibers. The XY translation stage is stationary during the printing of each object, moving only from object to object. Fig. 3 shows several examples of 3D printed structures: (a–c) straight walls made with PEO fiber, (d–e) cylinders made of a PEO-Ag nanoparticles composite, and more complex patterns, such as boxed scaffolds (f), triplets (g–h), flowers (i), as well as interdigitated (j) and single (k) microelectrodes. Some images are shown as SEM micrographs (panels b, c, e), but their widths are large enough to be resolved optically (600 µm for the walls and 8 µm for the cylinder). As an example, Fig. 3d shows an optical photo of a 29 µm wide cylinder.

The jet speed is computed for a 3D object much like for a 2D object: the product of fiber length $L$ printed in one period times the frequency $\nu$ of the jet-deflecting signal: $U_j = L\nu = L/T$. For the case of walls (Fig. 3a–c), two layers of fiber are deposited per period (20 ms). Therefore, the jet speed equals twice the wall length (0.6 mm) times the frequency of the jet-deflecting signal (50 Hz), namely 60 mm s$^{-1}$. For the case of the cylinder in Fig. 3e, the jet speed is equal to the diameter (0.008 mm) times $\pi$ and times the frequency of the jet-deflecting signal (100 Hz), namely 2.5 mm s$^{-1}$. Note that neither the object's height nor the number of fiber layers (up to 150 in the case of the walls) are used in the computation.

### 3.4. Influence from jet deflection parameters

Fig. 4a shows how the width of a 2D track varies with the jet deflection signal amplitude at constant frequency, on an EHD jet

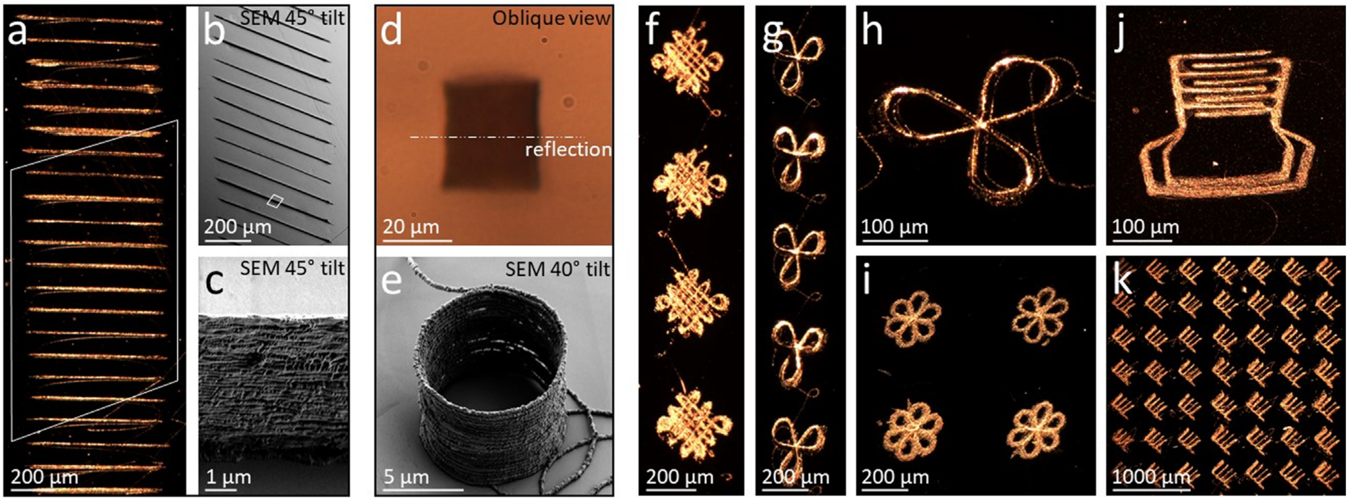


**Fig. 3.** The jet speed determination from the size of printed structures. Optical images (a, d, f–k) and SEM micrographs (b, c, e) of 3D printed structures on still Si wafer substrates by EHD jet-deflection, and which can be used for determining the jet speed: a–c) Straight walls with 50, 100, and 150 layers, printed by a 60 mm $s^{-1}$ jet using 50 Hz sawtooth signals (150 layers for (c)); (d–e) cylindrical structures of PEO and 50 nm Ag nanoparticles, where (d) shows a 100-layer cylinder printed at 200 Hz and at 18.2 mm $s^{-1}$ jet speed, and (e) a 25-layer cylinder printed at 100 Hz and 2.5 mm·s-1 jet speed; f–k) Complex patterns: boxed scaffolds (f), triplets (g–h), flowers (i), interdigitated electrodes (j) and separate electrodes (k), with jet-deflecting frequency at 12.5 Hz (j), 50 Hz (f, i, k), and 100 Hz (g, h). Inks used: 8% PEO 300 kDa in water: ethylene glycol (4:1) was used for (a–c) and (j), while 5% Ag NPs in 4.75% PEO 300 kDa in water:ethanol (1:3) for the rest. Glass tips were used as nozzle in all cases. Dry nitrogen was supplied around the nozzle for (d–e). Nozzle voltage ranged between 800 and 1200 V, and nozzle to collector distance was 3 mm.

moving at 140 mm $s^{-1}$ towards the collection substrate. At low speeds, the jet buckles over the collector, and the width of the fiber track, shown in Fig. 4b, increases linearly with amplitude (cases A through F). This corresponds to the *buckled jet regime* in Scheme 1b. Eventually, a critical condition is reached, represented on this graph as $\alpha$, for which the printed fiber is aligned, corresponding to the *matched speed regime* in Scheme 1b. As the signal amplitude increases beyond that for the critical condition, the fiber remains aligned, while track's width remains constant (cases G and H). This corresponds to the *stretched jet regime* in Scheme 1b. The constancy in pattern width arises probably because, beyond condition $\alpha$, the jet resists stretching as the electrical force acting on the jet due to the jet deflection signal is mostly transverse to the jet, becoming unable to develop any significant mechanical tension along the jet. Conceivably, an ink could be soft enough to yield under this electrical force, in which case the track's width would be expected to increase after point $\alpha$. Still, the critical condition would probably be detectable in the plot of the track's width versus amplitude by a change (decrease) in slope after $\alpha$. Fig. 4c illustrates how, at this signal frequency, the pattern width is expected to vary with the signal amplitude for different jet speeds. The sloped part of the curves, which corresponds to buckled fiber, is the same up to each critical point, which is attained at larger amplitudes for larger jet speeds.

Fig. 5 shows the role played by the frequency of the jet-deflecting signal, while keeping constant amplitude. When the frequency is low enough, the jet undergoes buckling, at condition A (50 Hz). As the frequency is raised, the extent of the buckling is reduced. Eventually, jet buckling disappears as the printed fiber becomes straight at the critical condition $\alpha$, reached between conditions A and B in Fig. 5b, and which corresponds to the *matched speed regime* (Scheme 1b). Beyond this condition, in the *stretched jet regime* (Scheme 1b) the track's width decreases with increasing frequency (conditions B-E), as imposed by mass conservation. Indeed, assuming a constant diameter fiber, the simple inverse dependence$W = U_j/(2v)$ fits the data well (Fig. 5b). The good agreement between theory and experiment suggests that the jet deflection did not cause fiber stretching (as concluded in Fig. 4b by a different argument).

### 3.5. Case study: Jet speed determination using 2D tracks in the presence of jet instabilities

The approach for determining jet speed was applied to detect instabilities in the EHD jetting causing jet speed pulsing or movement of jet ejection point. Fig. 6 displays two different situations, showing for each confocal microscopy images of 2D printed tracks and graphs of the corresponding jet speed, as obtained by our method, and the centerline position of the printed fiber track. In both cases, the track's width can be easily converted to jet speed, as twice the track's width times the jet deflection frequency ($U_j = 2Wv$). In Fig. 6a, the changing width of the track reflects a beating in the jet speed of about 1.2 Hz, while the jet is deflected at a much faster frequency (500 Hz). Fig. 6b shows a case in which a correlation exists between the centerline position of the printed pattern and its width, thus the jet speed. This is the result of a beating of the jet ejection point as shown in images of the ink drop in Fig. 6d, indicated by red and yellow arrows. In the case of Fig. 6a, for which the centerline position remained constant in time, the point of jet ejection on the drop did not beat, as demonstrated in Fig. 6c. The process of detecting the two types of jet instability shown in Fig. 6 can also be automated using *in situ* inspection equipment and image recognition software, and then be used for ensuring stable jetting conditions while printing.

### 3.6. In situ inspection system implementation

The method can be implemented using standard machine-inspection optics and image recognition software, to automatically detect the widths of the printed structure (both of 2D fiber tracks and 3D structures). Fig. 7 illustrates this, where the printed fiber tracks are imaged with a standard CMOS camera coupled to a conventional microscope using standard fiber optic illumination (see methods section). The jet was electrostatically deflected along a plane perpendicular to the direction of stage motion (Fig. 7a). The stage moved much slower than the jet speed, so that fiber was laid down nearly perpendicularly to the direction of substrate motion (Fig. 7b–d). The frequency and amplitude of the jet deflection signal were high enough to deposit fiber without buckling. As

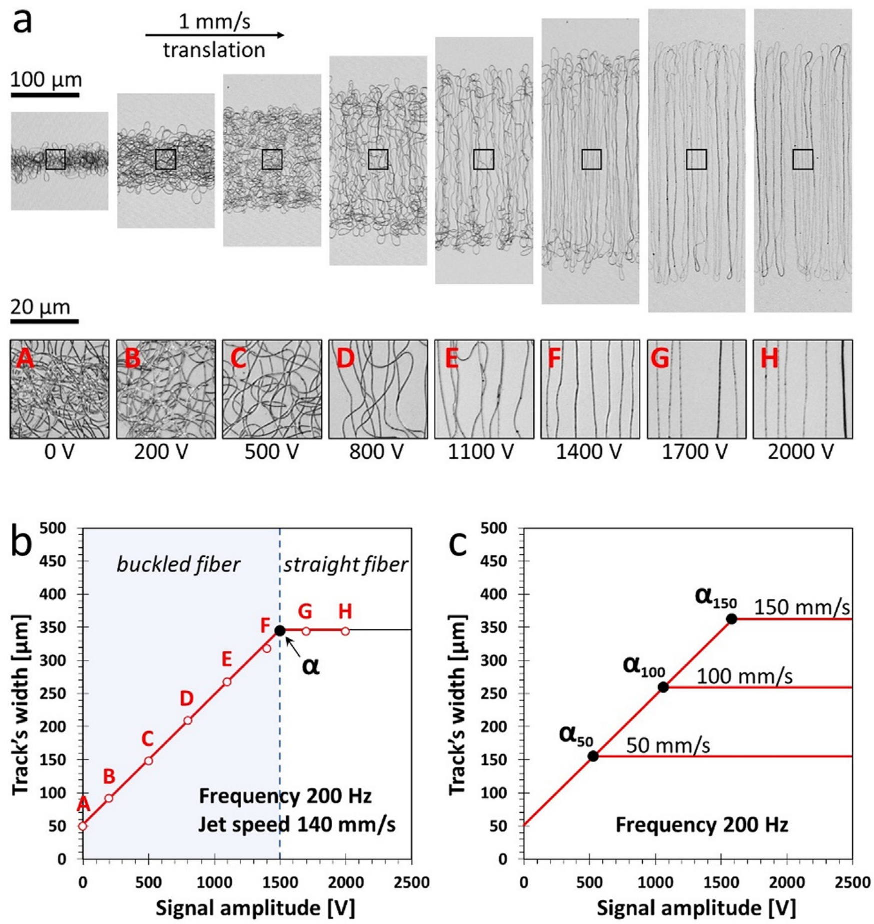


**Fig. 4.** Effect of the jet-deflecting signal amplitude on the width of a 2D pattern printed on a slow-moving substrate. (a) Confocal microscopy images of PEO fiber collected as the substrate moves at 1 mm $s^{-1}$ and the jet is deflected in the perpendicular direction with a sawtooth wave at 200 Hz, for different amplitudes of the jet-deflecting signal (values shown). (b) Dependence of the width of the printed fiber track on the signal amplitude at constant frequency, covering the different printing regimes. Buckled fiber is collected in the blue shaded zone, where the jet speed cannot be determined by the proposed method. (c) Printed track's width versus signal amplitude extrapolated from panel (b) at different fiber speeds. Ink: 3% PEO 1 MDa in water:ethanol (1:1). Syringe pump rate: 70 nL $min^{-1}$. Glass tip nozzle at 950–1100 V. Dry nitrogen gas was supplied around the jet. (For interpretation of the references to color in this figure legend, the reader is referred to the web version of this article.)

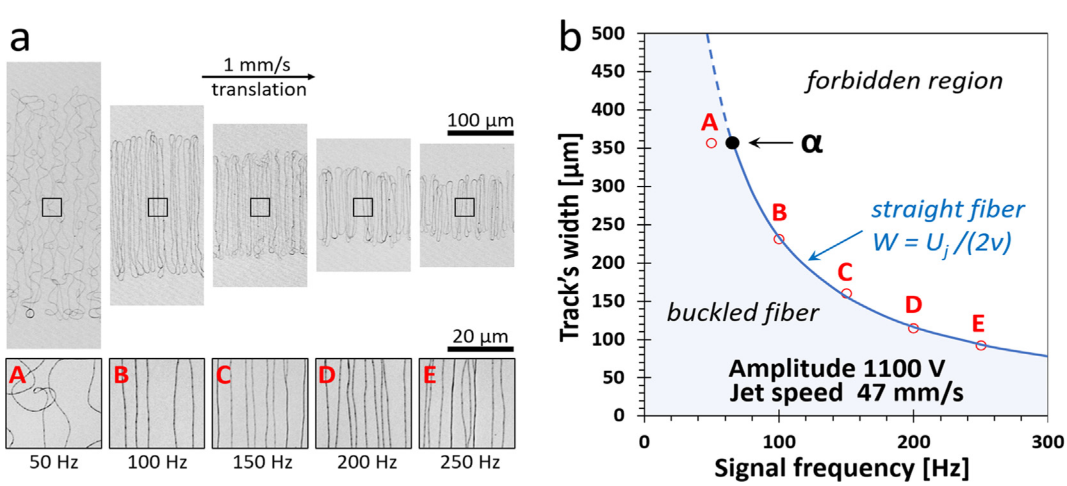


**Fig. 5.** Effect of the frequency ($\nu$) of the jet-deflecting signal on the width (W) of a printed pattern on a slow-moving substrate. (a) Confocal microscopy images of the PEO fiber collected while the substrate is moved at 1 mm $s^{-1}$ and the jet is deflected perpendicularly by a sawtooth signal for different frequencies of the jet-deflecting signal at fixed amplitude (1100 V). (b) Width of the printed fiber track versus frequency. The blue shaded area displays the region where the jet buckles and jet speed cannot be determined by the proposed method. Ink: 3% PEO 1 MDa in water:ethanol (1:1). Syringe pump rate: 70 nL $min^{-1}$. Glass tip nozzle at 950–1100 V. Dry nitrogen gas was supplied around the jet. (For interpretation of the references to color in this figure legend, the reader is referred to the web version of this article.)

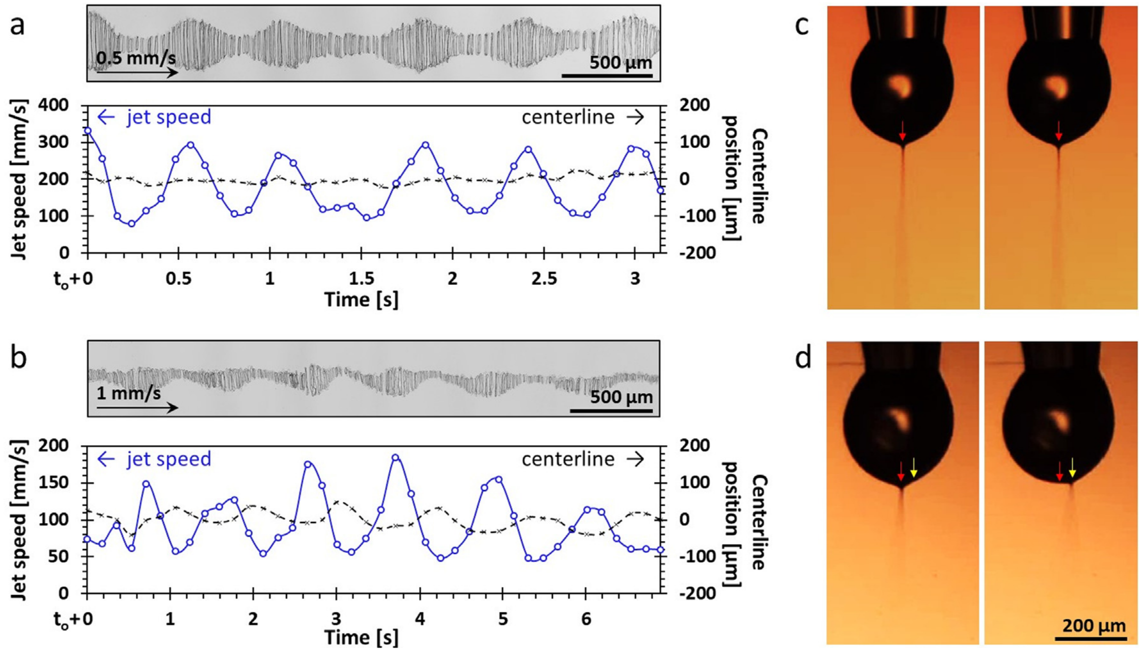


**Fig. 6.** Detection of jet instabilities. Jet instabilities occurred during PEO fiber collection on a moving substrate, while the jet was deflected in the perpendicular direction with a sawtooth signal at 500 Hz and 2000 V amplitude. (a–b) Confocal image of the fiber track and plot of the jet speed and track's centerline position for (a) jet with pulsating speed, and (b) jet pulsation with displacement of the jet on the pendant drop. (c–d) optical images of the pendant drop with EHD jet during printing corresponding to cases shown on (a–b), respectively. Arrows indicate the point of jet ejection. Nozzle voltage: 1000 V. Ink: 3% PEO (1 MDa) in water:ethanol (1:1). Syringe pump rate: 50 nL·min$^{-1}$. Dry nitrogen gas was supplied around the jet.

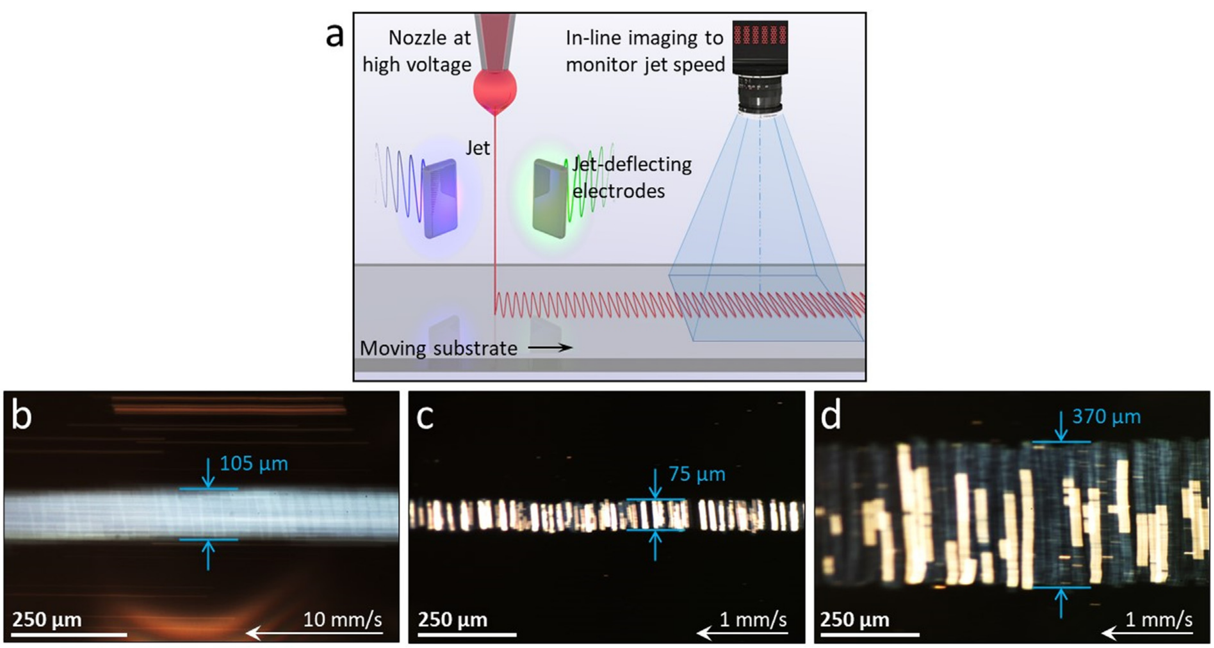


**Fig. 7.** In situ monitoring of the jet speed via the width of a printed fiber track. Schematic (a) and top-view optical photographs (b–d) of PEO fiber tracks collected while the substrate moves sideways, and the jet is deflected in the perpendicular direction with a sawtooth signal, with frequencies and amplitudes of: (b) 200 Hz and 1200 V, (c) 250 Hz and 1100 V, and (d) 50 Hz and 1100 V. The photographs were taken with a CMOS camera with the same substrate speed as used during printing. Exposure times: (b) 50 ms, (c) 10 ms and (d) 25 ms. Deposition conditions: (b) is the same as case C in Fig. 2b, and (c) and (d) are close to Fig. 5 cases E and A, respectively, but with a slower jet (leading to straight fibers). The computed jet speeds were: (b) 42, (c) 37.5, and (d) 37 mm s$^{-1}$.

the fiber is straight and perfectly aligned, the jet speed is computed as the product of twice the width of the track times the frequency of the jet-deflecting signal. The computed jet speeds for Fig. 7b–c were: (b) 42 mm s$^{-1}$, (c) 37.5 mm s$^{-1}$, and (d) 37 mm s$^{-1}$.

As the track's width can be optically determined using a standard camera, this method does not rely on resolving individual fibers and does not require expensive microscopy nor laborious analysis. Fig. 7b used 10 mm s$^{-1}$ substrate speed, producing a blurred image, while Fig. 7c and d used a lower speed of 1 mm s$^{-1}$, resolving individual fiber tracks. The shiny (golden) lines visible in this case result from stronger scattering from multiple fibers stacked on top of each other by self-assembly (as explained earlier). The track's width, however, is independent of the extent of self-assembled fiber under these conditions. Note also that in Fig. 7b the substrate travels 500 μm during the exposure time, so the illusion of individual fibers may result from aliasing of the printing frequency (200 Hz) with the LED light source frequency (50 Hz).

### 3.7. Practical application

As noted in the introduction, before starting the printing process or when changing a parameter of the system, the speed of the jet generated from the specifically used ink, printing parameters, and environmental conditions need to be determined to adapt the printing speed by adjusting the movement of the stage (when a stage is used to create a pattern) or the jet deflection signal (when jet deflection is used). Once the printing process has started, the *in situ* and inline measurement of the jet speed can be used for a better control of the EHD printing process, enabling additional adjustment of the dimensions of the printed object, and detecting and compensating for instabilities in the printing system, the ink, or the environment.

By way of example, Fig. 8a shows a pair of interdigitated electrodes produced using the stage movement to define the electrode shape and jet deflection to adjust the width of the electrode arms. The jet speed during the printing of this electrode was 170 mm $s^{-1}$. The EHD printing parameters and thus the jet speed can be intentionally modified during the printing process to produce electrodes with different size and geometry, but also with different arm width, different electrode microstructure, amount of material deposited, and thickness of the deposited fiber. Besides, the printing speed could be maximized after taking into account the size and precision required for the object to be printed, to minimize production time. The minimum time required to print each object, and also the printing precision and repeatability, depend on the jet speed. It could be of interest to print objects of different sizes in the same process or objects with features that require different printing precision. Conveniently, this jet speed can be rapidly adjusted by just modifying the jet ejection voltage. However, owing to the complex interrelation between the several parameters influencing it, the easiest and most precise strategy to continuously match jet and printing speeds is to frequently measure the former to subsequently adjust the latter. On the other hand, during the printing process, the speed of the jet may also vary unintentionally due to variations in the process or environmental parameters, e.g. a change in ambient temperature or humidity. As an example, a moderate change of relative humidity from 60 to 65% results in a large increase of the speed of the jet from 71 mm $s^{-1}$ to 146 mm $s^{-1}$, as measured using our jet-deflection strategy. When the jet speed is measured *in situ*, this information can be used as feedback for the real-time adjustment of the printing parameters to correct the jet speed or for the real-time adjustment of the printing speed, defined by the movement of the stage (in stage-driven printing) or the frequency of the jet deflection (in jet-deflection printing), to compensate for the change of external parameters.

Fig. 8b displays the same interdigitated electrodes as in Fig. 8a but printed with a lower jet speed, 115 mm $s^{-1}$. In this case, the lower jet speed was not related to a change of any external parameter, but it resulted from a decrease of the nozzle voltage. Notice that if no additional process parameter is modified, the arm width of the new electrode is strongly reduced, which would significantly change the characteristics of the electronic device. Larger changes in the jet speed could result in further deterioration of the printed object due to fiber bucking or fiber stretching, as discussed in the introduction. Our method allows to rapidly determine the jet speed, to either adjust it to return to the previous value (by changing nozzle voltage if the jet speed was unintentionally modified by a change of relative humidity, for example) or to adjust the printing parameters to recover the desired object characteristics. In Fig. 8c we display the same interdigitated electrodes, obtained with the same nozzle voltage as in Fig. 8b, but printed after adjusting the process parameters, in this case the jet deflection frequency and stage speed, to accumulate the same amount of fiber, thus

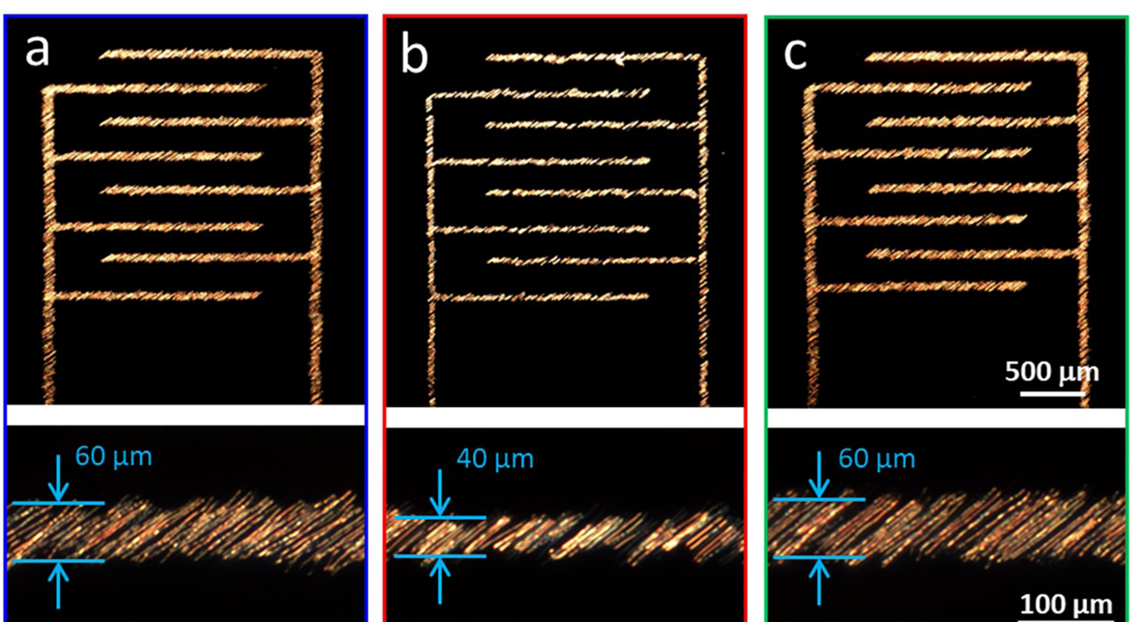


**Fig. 8.** Interdigitated electrodes printed using the XY stage translation to define their geometry and jet deflection to define their arm width. (a) Electrodes printed using a nozzle voltage $V_N$ = 700 V, a jet speed $U_J$ = 170 mm $s^{-1}$, a deflection frequency of $\nu$ = 1000 Hz, and a stage speed $U_s$ = 4 mm $s^{-1}$. (b) Thinner electrodes obtained when reducing the jet speed through a decrease of the nozzle voltage: $V_N$ = 630 V, $U_J$ = 115 mm $s^{-1}$, $\nu$ = 1000 Hz, $U_s$ = 4 mm $s^{-1}$. Notice that a similar change would be obtained when reducing the ambient relative humidity, for example. (c) Electrodes with recovered geometric parameters and fiber density produced by adjusting the deflection frequency and stage speed to the new jet speed. $V_N$ = 630 V, $U_J$ = 115 mm $s^{-1}$, $\nu$ = 670 Hz, $U_s$ = 2.7 mm $s^{-1}$. Dry nitrogen gas was supplied around the jet.

compensating for the jet speed change. By doing so, the initial electrode arm dimensions and internal geometry were recovered.

The proposed method allows for *in situ* and inline jet speed determination to EHD printing. Importantly, the method can be easily implemented in an EHD printer regardless of whether or not the printer uses jet deflection during the printing (although jet deflection is used in the determination of jet speed). While the present work provided a proof-of-concept, explored the opportunities and proposed the regimes at which this approach is best practiced, further work is required for the implementation and validation of the *in situ* monitoring system. Further work includes the development of proper illumination and capturing of the printed pattern, as well as an algorithm for image recognition and computation of the jet speed discussed above. Image analysis is typically done by applying a threshold to convert obtained images into black-and-white to enhance accuracy. Fiber track width can be then computed by calculating the number of pixels representing the fiber track. Preferably, the width of the fiber track and the centerline position can be determined through detecting the edges of a fiber track, similarly to Fig. 6a–b, ultimately allowing not only the *in situ* monitoring of the jet speed, but also of the stability/displacement of the jet ejection point on the pendant drop. Depending on the size and complexity of printed objects, such image recognition may be used even continuously.

Once the jet speed is computed, these data may be used for the feedback loop control of the printing process. As printing speed and jet speed must be matched for printing with high fidelity, two options exist. One is controlling the jet speed via such parameters as nozzle voltage or ink supply rate for bringing the jet speed to its preset value. The opposite strategy would be to adjust the jet deflection parameters such that the printing speed would match the new jet speed. To find proper jet deflection parameters, first the desired motif and its size must be selected, which allows computing the fiber length going into one layer. Practically, this is easily achieved in our custom-made software, which computes a "perimeter" dimensionless number, representing the length of the motif divided by the length of its size in X or Y dimension (e.g., such a number equals 4 for a square and to $\pi$ for a circle, etc.). Then, multiplying this dimensionless number by the desired size of a printed motif (e.g., 0.2 mm), the length of the fiber needed for printing one layer is obtained. Then, deflection frequency is computed by dividing the specific jet speed by the fiber length needed for one layer. Finally, for the computed frequency, the deflection amplitude must be chosen which provides the necessary jet deflection angle [10]. We point out that successful implementation of the proposed method for the *in situ* speed monitoring and automated control in a feedback loop would require extensive parametric study of the jet deflection process, as well as subsequent optimization of an algorithm matching those speeds. Considering that this method enables measuring the jet speed multiple times per second, it will prove priceless for generating data sets free of human error and bias for high-throughput analysis of multiple printing parameters and ink compositions on the jet speed and stability. Future advancement of NFES requires more automation of the printing process and is dependent on the capability to monitor the EHD jet stability and arrival speed *in situ*. As the present work enables a simple method to compute the jet speed from the width of fiber tracks, it opens fascinating opportunities for the future automation of NFES.

## 4. Conclusions

Additive manufacturing by near-field electrospinning is based on printing small EHD jets as continuous fibers. Owing to the small fiber width and high jet speeds achieved by this method, high resolution is combined with high printing speed. Printing with high fidelity depends critically on controlling the jet arrival speed. Here we proposed a suitable strategy to determine jet arrival speed based on deflecting the jet electrostatically. Thanks to such deflection, the position of the contact point where the jet meets the substrate is controlled independently from the motion of the substrate. This may allow for higher speed printing and freedom to print complex predefined 2D patterns and 3D objects than are possible by moving stages.

To determine jet speed via jet-deflection, a periodic motif was printed either into a 2D pattern, by moving the substrate under the nozzle, or a 3D structure, by keeping the substrate still. The width of wavy 2D patterns reached an asymptotic value as the substrate speed decreased and the zig-zag pattern became substantially orthogonal to the direction of the substrate motion. Jet buckling was avoided by using a high enough amplitude and frequency of the jet deflecting signal. The width of the printed pattern reached an asymptotic value as either the amplitude or the frequency increased, beyond the critical condition where the fiber went from a buckled pattern to becoming "straight". At any such conditions leading to unbuckled fiber, jet speed could be readily computed from the product of the frequency of the deflection signal and the width of the periodically printed pattern (times a factor which depends on the printed geometry). A similar approach was used to determine jet speed by analyzing the size (width) of 3D structures (e.g. cylinders or walls), so long as the fiber printing was driven by the jet deflection signal and was not caused by its buckling over the substrate. In the terminology introduced in Scheme 1, the method can be practiced in the *matched speed regime* as well as, by using excess amplitude or frequency in the jet-deflecting signal, in the *stretched jet regime*. We applied this method to a case study, showing the occurrence of jet instabilities during printing. Finally, we demonstrated the feasibility to determine the fiber speed *in situ* during printing, using inexpensive optical equipment, and by automated image recognition software. In this regard, this method is far superior to previous methods, for which determining the jet speed involves laborious *ex situ* high-resolution imaging of individual nanofibers. The new approach does not require a fast-moving translation stage to attain speeds comparable to the jet speed, as it works robustly with any desired stage speeds (even zero speed). Therefore, the new approach can handle jets that move faster than state-of-the-art translation stages.

## Data availability

Original measurement data are available upon reasonable request.

## CRediT authorship contribution statement

**Ievgenii Liashenko:** Conceptualization, Investigation, Software, Data curation, Visualization, writing original draft. **Alberto Ramon:** Investigation, Data curation. **Andreu Cabot:** Supervision, Resources, Funding acquisition, writing original draft and editing final manuscript. **Joan Rosell-Llompart:** Supervision, Resources, Funding acquisition, writing original draft and editing final manuscript.

## Declaration of Competing Interest

The authors declare that they have no known competing financial interests or personal relationships that could have appeared to influence the work reported in this paper.

## Acknowledgements

This work was supported by the Spanish Ministerio de Ciencia e Innovación (MCI), the Agencia Estatal de Investigación (AEI) and the Fondo Europeo de Desarrollo Regional (FEDER) through project PGC2018-099687-B-I00, and by Generalitat de Catalunya (Agència de Gestió d'Ajuts Universitaris i de Recerca - AGAUR) through projects 2017SGR1246, 2017SGR1516 and 2019INNOV00054. A. R. acknowledges financial support from Ministerio de Ciencia, Innovación y Universidades through FPI fellowship BES-2017-081681.


## Appendix A. Supplementary material

Supplementary data to this article can be found online at https://doi.org/10.1016/j.matdes.2021.109791.

## References


[1] S. Huang, N. Bu, Y. Duan, Y. Pan, H. Liu, Z. Yin, Y. Xiong, Electrohydrodynamic direct-writing, Nanoscale 5 (2013) 12007–12017, https://doi.org/10.1039/c3nr04329k.

[2] M.S. Onses, E. Sutanto, P.M. Ferreira, A.G. Alleyne, J.A. Rogers, Mechanisms, capabilities, and applications of high-resolution electrohydrodynamic jet printing, Small 11 (2015) 4237–4266, https://doi.org/10.1002/smll.201500593.

[3] J. Schneider, P. Rohner, D. Thureja, M. Schmid, P. Galliker, D. Poulikakos, Electrohydrodynamic nanodrip printing of high aspect ratio metal grid transparent electrodes, Adv. Funct. Mater. 26 (2016) 833–840, https://doi.org/10.1002/adfm.201503705.

[4] B. Zhang, J. He, X. Li, F. Xu, D. Li, Micro/nanoscale electrohydrodynamic printing: from 2D to 3D, Nanoscale. 8 (2016) 15376–15388, https://doi.org/10.1039/c6nr04106j.

[5] D. Ye, Y. Ding, Y. Duan, J. Su, Z. Yin, Y.A. Huang, Large-scale direct-writing of aligned nanofibers for flexible electronics, Small 14 (2018) 1703521, https://doi.org/10.1002/smll.201703521.

[6] T.M. Robinson, D.W. Hutmacher, P.D. Dalton, The next frontier in melt electrospinning: taming the jet, Adv. Funct. Mater. 29 (2019) 1904664, https://doi.org/10.1002/adfm.201904664.

[7] W. Wang, P.N. Stipp, K. Ouaras, S. Fathi, Y.Y.S. Huang, Broad bandwidth, self-powered acoustic sensor created by dynamic near-field electrospinning of suspended, transparent piezoelectric nanofiber mesh, Small 16 (2020) 2000581, https://doi.org/10.1002/smll.202000581.

[8] M. Castilho, R. Levato, P.N. Bernal, M. de Ruijter, C.Y. Sheng, J. van Duijn, S. Piluso, K. Ito, J. Malda, Hydrogel-based bioinks for cell electrowriting of well-organized living structures with micrometer-scale resolution, Biomacromolecules 22 (2021) 855–866, https://doi.org/10.1021/acs.biomac.0c01577.

[9] J. Rosell-Llompart, J. Grifoll, I.G. Loscertales, Electrosprays in the cone-jet mode: from Taylor cone formation to spray development, J. Aerosol Sci. 125 (2018) 2–31, https://doi.org/10.1016/j.jaerosci.2018.04.008.

[10] I. Liashenko, J. Rosell-Llompart, A. Cabot, Ultrafast 3D printing with submicrometer features using electrostatic jet deflection, Nat. Commun. 11 (2020) 753, https://doi.org/10.1038/s41467-020-14557-w.

[11] D. Shin, J. Kim, S. Choi, Y. Lee, J. Chang, Droplet-jet mode near-field electrospinning for controlled helix patterns with sub-10 μm coiling diameter, J. Micromech. Microeng. 29 (2019) 45004, https://doi.org/10.1088/1361-6439/ab025e.

[12] D. Sun, C. Chang, S. Li, L. Lin, Near-field electrospinning, Nano Lett. 6 (2006) 839–842, https://doi.org/10.1021/nl0602701.

[13] A. Greiner, J.H. Wendorff, Electrospinning: a fascinating method for the preparation of ultrathin fibers, Angew. Chemie Int. Ed. 46 (2007) 5670–5703, https://doi.org/10.1002/anie.200604646.

[14] X.X. He, J. Zheng, G.F. Yu, M.H. You, M. Yu, X. Ning, Y.Z. Long, Near-field electrospinning: progress and applications, J. Phys. Chem. C 121 (2017) 8663–8678, https://doi.org/10.1021/acs.jpcc.6b12783.

[15] P. Fisch, M. Holub, M. Zenobi-Wong, Improved accuracy and precision of bioprinting through progressive cavity pump-controlled extrusion, Biofabrication 13 (2020) 015012, https://doi.org/10.1088/1758-5090/abc39b.

[16] J. Go, A.J. Hart, Fast desktop-scale extrusion additive manufacturing, Addit. Manuf. 18 (2017) 276–284, https://doi.org/10.1016/j.addma.2017.10.016.

[17] D. Shin, J. Kim, J. Chang, Experimental study on jet impact speed in near-field electrospinning for precise patterning of nanofiber, J. Manuf. Process. 36 (2018) 231–237, https://doi.org/10.1016/j.jmapro.2018.10.011.

[18] M. Gamero-Castaño, The structure of electrospray beams in vacuum, J. Fluid Mech. 604 (2008) 339–368, https://doi.org/10.1017/S0022112008001316.

[19] I. Liashenko, A. Hrynevich, P.D. Dalton, Designing outside the box: unlocking the geometric freedom of melt electrowriting using microscale layer shifting, Adv. Mater. 32 (2020) 2001874, https://doi.org/10.1002/adma.202001874.

[20] A. Hrynevich, I. Liashenko, P.D. Dalton, Accurate prediction of melt electrowritten laydown patterns from simple geometrical considerations, Adv. Mater. Techn. 5 (2020) 2000772, https://doi.org/10.1002/admt.202000772.

[21] T. Han, D.H. Reneker, A.L. Yarin, Buckling of jets in electrospinning, Polymer (Guildf) 48 (2007) 6064–6076, https://doi.org/10.1016/j.polymer.2007.08.002.

[22] N.M. Ribe, M. Habibi, D. Bonn, Liquid rope coiling, Annu. Rev. Fluid Mech. 44 (2011) 249–266, https://doi.org/10.1146/annurev-fluid-120710-101244.

[23] S. Chiu-Webster, J.R. Lister, The fall of a viscous thread onto a moving surface: a 'fluid-mechanical sewing machine', J. Fluid Mech. 569 (2006) 89–111, https://doi.org/10.1017/S0022112006002503.

[24] Y. Duan, Y. Ding, Z. Xu, Y. Huang, Z. Yin, Helix electrohydrodynamic printing of highly aligned serpentine micro/nanofibers, Polymers (Basel). 9 (2017) 434, https://doi.org/10.3390/polym9090434.

[25] H.-Y. Kim, M. Lee, K.J. Park, S. Kim, L. Mahadevan, Nanopottery: coiling of electrospun polymer nanofibers, Nano Lett. 10 (2010) 2138–2140, https://doi.org/10.1021/nl100824d.

[26] X. You, C. Ye, P. Guo, Electric field manipulation for deposition control in near-field electrospinning, J. Manuf. Process. 30 (2017) 431–438, https://doi.org/10.1016/j.jmapro.2017.10.005.

[27] J. Kim, D. Shin, K.-B. Han, J. Chang, A quantification of jet speed and nanofiber deposition rate in near-field electrospinning through novel image processing, J. Micro Nano-Manufacturing. 6 (2018) 031002, https://doi.org/10.1115/1.4039794.

[28] T.D. Brown, P.D. Dalton, D.W. Hutmacher, Melt electrospinning today: an opportune time for an emerging polymer process, Prog. Polym. Sci. 56 (2016) 116–166, https://doi.org/10.1016/j.progpolymsci.2016.01.001.

[29] G. Hochleitner, A. Youssef, A. Hrynevich, J.N. Haigh, T. Jungst, J. Groll, P.D. Dalton, Fibre pulsing during melt electrospinning writing, BioNanoMaterials 17 (2016) 159–171, https://doi.org/10.1515/bnm-2015-0022.

[30] N.G. Bastús, F. Merkoçi, J. Piella, V. Puntes, Synthesis of highly monodisperse citrate-stabilized silver nanoparticles of up to 200 nm: kinetic control and catalytic properties, Chem. Mater. 26 (2014) 2836–2846, https://doi.org/10.1021/cm500316k.

[31] G.S. Bisht, G. Canton, A. Mirsepassi, L. Kulinsky, S. Oh, D. Dunn-Rankin, M. Madou, Controlled continuous patterning of polymeric nanofibers on three-dimensional substrates using low-voltage near-field electrospinning, Nano Lett. 11 (2011) 1831–1837, https://doi.org/10.1021/nl2006164.

[32] P. Galliker, J. Schneider, H. Eghlidi, S. Kress, V. Sandoghdar, D. Poulikakos, Direct printing of nanostructures by electrostatic autofocussing of ink nanodroplets, Nat. Commun. 3 (2012) 890, https://doi.org/10.1038/ncomms1891.